Korea-Australia Rheology Journal
Vol. 13, No. 3, September 2001 pp. 109-123

Stress jump: experimental work and theoretical modeling

Ning Sun and Daniel De Kee*
Department of Chemical Engineering Tulane University New Orleans, LA 70118, U.S.A.
(Received October 10, 2000; final revision received April 23, 2001)

Abstract

A stress jump, defined as the instantaneous gain or loss of stress on startup or cessation of a deformation, has been predicted by various models and has relatively recently been experimentally observed. In 1993, Liang and Mackay measured shear stress jump data of xanthan gum solutions, and in 1996, Orr and Sridhar reported extensional stress jump data of Boger fluids. Shear stress jumps of suspensions and liquid crystal polymers have also been observed. In this contribution, experimental work as well as a variety of theoretical models, which are able to predict a stress jump, are reviewed.

1. Introduction

The last decade has seen a renewed and increasing interest in the stress jump phenomenon. It is defined as the instantaneous finite change in stress due to an instantaneous change in deformation rate. Such discontinuities were predicted by De Kee and Carreau (1979) and measured by Liang and Mackay (1993).

We identify three types of stress: a purely elastic stress as described by Hooke's law; a purely viscous stress as observed with Newtonian fluids and a viscoelastic stress associated with a relaxation time or spectrum. The stress jump is associated with the purely viscous contribution of the stress. As observed with Newtonian fluids, the stress is immediately established or dissipated upon startup or cessation of flow respectively. To characterize a viscoelastic stress, one can for example consider the mechanical analog of the Maxwell model. Even though the force associated with the dashpot is purely viscous in nature, it is coupled with an elastic spring force and thus the Maxwell model does not predict a stress jump, nor does any other similar viscoelastic model. However, the Voigt-Kelvin model, with a dashpot and a spring connected in parallel and assuming the elastic and viscous stresses to be independent, does predict a stress jump.

There are two possible mechanisms to account for a stress jump; a viscous intermolecular force and a viscous intramolecular force. The former force arises from the interaction between solvent molecules and polymer molecules and was used in the rigid dumbbell model (Bird *et al.*, 1987) and in the De Kee - Carreau model (De Kee and Carreau, 1979), to name just two. The latter force relies on the idea of an internal viscosity (Manke and Williams, 1987; 1992). The internal viscosity was first suggested by Kuhn and Kuhn (1945), and in the 1980s, the internal viscosity idea began to be associated with stress jump in the bead-rod-spring molecular model.

The stress jump has long been predicted by various models as scientists realize the coexistence of the purely viscous stress and viscoelastic stress in polymer solutions/melts and suspensions. Simulation work (Foss and Brady, 2000) has also been performed to identify the behaviors of different stress contributions, as shown in Fig. 1. In the

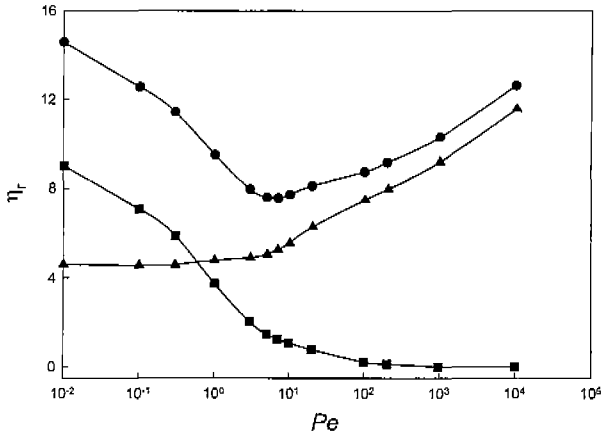

Fig. 1. Peclet number dependence of the different contributions to the relative viscosity of hard-sphere suspensions determined by Stokesian Dynamics. (From Foss and Brady, 2000, reprinted with permission from Brady), –●–; η_r (Total), –▲–; η_H (Hydrodynamic/viscous contribution), –■–; η_B (Brownian/elastic contribution).

*Corresponding author:ddekee@mailhost.tcs.tulane.edu

context of fluids, the purely elastic stress does not exist (except for visco-plastic materials) and the viscoelastic stress is sometimes referred to as the elastic-like stress or even elastic stress. We use elastic or elastic-like stress to indicate viscoelastic stress. Generally, the extra stress tensor is expressed as the sum of the elastic-like component $\underline{\underline{\sigma}}^e$ and the viscous component $\underline{\underline{\sigma}}^v$:

$$\underline{\underline{\sigma}} = \underline{\underline{\sigma}}^e + \underline{\underline{\sigma}}^v \quad (1)$$

Note that, $\underline{\underline{\sigma}}^v$ in Equation (1) may include the contribution from the viscous solvent as well as the contribution from polymer molecules. However, experimentalists were not able to distinguish the elastic from the viscous components until Mackay and coworkers developed a technique to measure the shear stress jump in early 1990's. Subsequently, a stress jump in extensional flow has also been observed (Orr and Sridhar, 1996; Spiegelberg and McKinley, 1996).

2. Experimental techniques

2.1. Shear rheometry

Stress jump measurements are difficult to execute, as the instrumentation is required to be able to capture the instantaneous changes of stress and distinguish them from all kinds of noise. The rheometer must be rate-controlled. Mackay *et al.* (1992) investigated instrument effects on stress jump measurements at cessation of flow. Two aspects were addressed in their paper. One dealt with the analog filters installed in most commercial rheometers and the other one dealt with the torque head inertia.

Analog filters serve to eliminate high frequency noise in torque signals. However, they also filter out useful stress jump signals and generate false smooth transient profiles. Mackay *et al.* (1992) set up a switch on their rheometer which enables measurements with or without filter. Basically, they illustrated the filter effect by comparison experiments and by simulation work. A Newtonian oil was used for stress relaxation tests. Ideally, the measured stress should instantaneously jump to zero. However, a smooth continuous stress relaxation curve in the first 30 ms was obtained due to the action of the filter. Without filter, substantial noise was present, and much faster stress decay was observed. They also considered a digital filter to mimic the behavior of the analog filter used in the rheometer. The digital filter was associated with the simulation work. The digital filter, represented by a set of equations, was able to generate output information identical to that measured using an analog filter, based on input data measured without the analog filter. In the simulation, stress relaxation results of an Oldroyd-B fluid model were compared with those filtered by the digital filter. Since the digital filter behaved as the analog filter, the simulation can be viewed as a substitution of testing the analog filter in the absence of noise. It was shown that the stress jump inherent to the Oldroyd-B model was completely removed with the digital filter.

Mackay *et al.* (1992) also studied the torsion spring technique, where the torque was calculated by measuring the spring angle displacement and the force rebalance technique, where a DC motor drove the shaft to a null position on a feed-back principle. In a rate-controlled rheometer, generally the lower tool rotates and the torque is measured on the upper tool. For a torsion spring type instrument, upon cessation of flow, the lower tool is assumed to stop immediately, while the upper tool tends to return to the equilibrium position and imposes an additional shear on the sample. Mackay *et al.* (1992) showed that such a shear, although small, causes the spring to return smoothly and prevents accurate measurements of stress jump. A force rebalance type instrument is able to measure a stress jump, as the torque head remains at the equilibrium position through constant updating by the feed-back system.

The rheometer used by Mackay and his coworkers was a modified RFS rheometer (Rheometrics, NJ, USA). The torque transducer used the force rebalance technique. When determining a stress jump, the sample was first sheared sufficiently long to reach steady state. After the shear was stopped, a high sampling frequency was used for the first second (512 Hz) and a much lower one was used for the remainder of the experiment. The short time transient measurements were taken with the internal analog filter off and the scatter in the data was smoothed by taking the measurements four times, two in the clockwise direction and two in the counter-clockwise direction. The primary data (the average of the four measured values) was further processed with a Butterworth digital filter to eliminate high-frequency noise. Due to some inevitable instrument effects as revealed by testing Newtonian fluids, the data collected in the first 15-20 ms were ignored. Subsequent data were extrapolated to the instant of cessation to obtain the retained elastic-like stress values. Two extrapolation procedures were used: the log of stress versus linear time and a linear stress versus time approach. Essentially equivalent values were obtained with these two procedures.

2.2. Extensional rheometry

The extensional rheometers used were described in detail by Tirtaatmadja and Sridhar (1993) and by Orr and Sridhar (1996). Basically, two platforms were mounted on a shaft. The platforms can move either independently with a servo controller connected to each one of them, or simultaneously with a servo motor connected to the shaft. A force transducer (Cambridge Technology 400A) was attached to one of the platforms whilst a fixture was attached to the other. The diameter of the filament during stretching was measured by an optical diameter-measuring device (Zumbach ODAC). When both platforms were moving, the Zumbach

was placed at the mid-point of the filament. If only one platform was moving, the Zumbach was offset from the mid-point of the filament to avoid the effect of the end plates. The analog force transducer signals were collected into a computer via an analog-to-digital card (ADC). To enable the capture of fast transients, the cut-off frequency of analog filters was increased to 40 Hz because it was found that this frequency represented a nice compromise between signal quality and lag due to filtering.

2.3. Experimental results

2.3.1. Shear stress jump

To our knowledge Mackay and coworkers were the only group performing mechanical measurements of shear stress jump (Mackay, 1999). They have investigated viscous-like and elastic-like components of shear stress for several systems, including suspensions, polymer solutions and rigid molecule systems such as viruses and liquid crystal polymers (LCP).

A dimensionless stress jump ratio at cessation of flow was defined as (Liang and Mackay, 1993):

$$R^{-}(t;\gamma_s,\dot{\gamma}_s)=\frac{\sigma_s^{-}(t;\gamma_s,\dot{\gamma}_s)}{\sigma_s(\dot{\gamma}_s)-\eta_{(s)}\dot{\gamma}_s} \tag{2}$$

where $\eta_{(s)}$ is the measured solvent viscosity, t is the time after cessation of shear and γ_s refers to the strain achieved during shearing at the rate $\dot{\gamma}_s$, prior to cessation of flow. $\sigma_s(\dot{\gamma}_s)$ represents the steady state shear stress while σ_s^{-} refers to the transient shear stress after cessation of flow. The contribution of the Newtonian solvent or the continuous medium is excluded.

2.4. Suspensions

In 1995, Mackay and Kaffashi (1995) studied the shear properties of highly deionized polystyrene spheres in water. The particle diameter size was 111.6± 2.8 nm, determined by SEM and dynamic light scattering (DLS). Four suspensions were produced, with volume fractions of 0.246, 0.256, 0.383 and 0.419 respectively. All suspensions were iridescent at rest, indicating that they had a crystal-like mesostructure. A 25-mm diameter cone and plate with an angle of 0.09974 rad was employed for the rheological measurements. They determined that the stress jump ratio at cessation of flow (at t=0) for the four samples decreased with increasing shear rate. The $R^{-}-\dot{\gamma}$ evolution for the four different volume fraction samples, appeared close to each other, as shown in Fig. 2. The stress jump ratio at a shear rate of 0.1 s^{-1} was around 0.95, while at 300 s^{-1} it was around 0.25. This confirmed that the elastic-like stress was dominant at low shear rates while viscous stress was dominant at high shear rates. They attributed this change in the relative contribution of these two stresses to possible shifts in the microstructure. The magnitudes of the stresses showed strong concentration dependence. The viscous

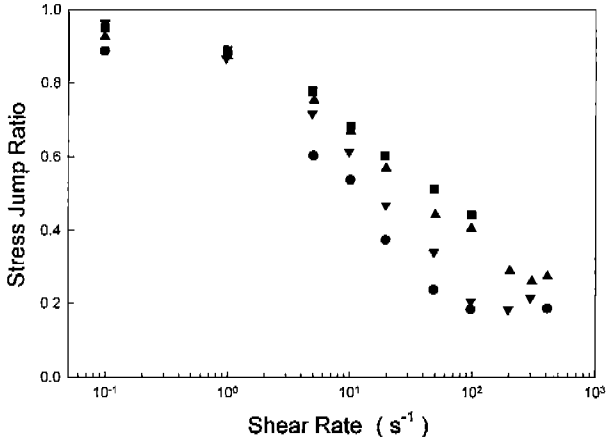

Fig. 2. Shear rate dependence of the stress jump ratio upon cessation of shear flow for four polystyrene sphere suspensions. (Data adapted from Mackay and Kaffashi, 1995), ▼ ; 0.246 (volume fraction), ●; 0.256, ▲; 383, ■; 0.419.

stress displayed a more severe dependence on volume fraction at high shear rate than at low shear rate. This was also related to the change in microstructure.

In 1997, Kaffashi *et al.* (1997) studied the shear properties of Brownian, rigid sphere suspensions. The polymethylmethacrylate (PMMA) spheres were modified with about 10% styrene, crosslinked with divinyl benzene and stabilized by a chemically grafted solvated layer of poly (12-hydroxystearic acid). The mean hydrodynamic particle diameter was 376 nm, measured via DLS and the mean dried particle diameter was 316 nm, measured via electron microscopy. The solvated layer was taken into account for calculating the effective volume fraction. Three samples were used, with effective volume fractions (volume fractions) 0.547 (0.456), 0.586 (0.488) and 0.688 (0.573). The geometry used for the measurements was a 50 mm diameter cone and plate with a cone angle of 0.0874 rad. The limited shear rate range used in this study (0.1 s^{-1} to 60 s^{-1}) did not reveal shear thickening. It was found that the viscous viscosity component remained almost constant with shear rate, while the elastic-like one was shear-thinning over the whole shear rate range, with a power law index of approximately zero. The relative viscosity versus shear rate for the 0.547 volume fraction is shown in Fig. 3. The elastic-like stress for the lowest volume fraction showed a local maximum with shear rate while for the highest volume fraction it was a monotonically increasing function of shear rate. The behavior of the intermediate one was between the other two. Such phenomena were believed to indicate that the various volume fractions used in the study had different structural responses to shear. Furthermore, the relaxation of the elastic-like stress was found to fit a power law. Analysis of the data yielded a unique time constant for all volume fractions

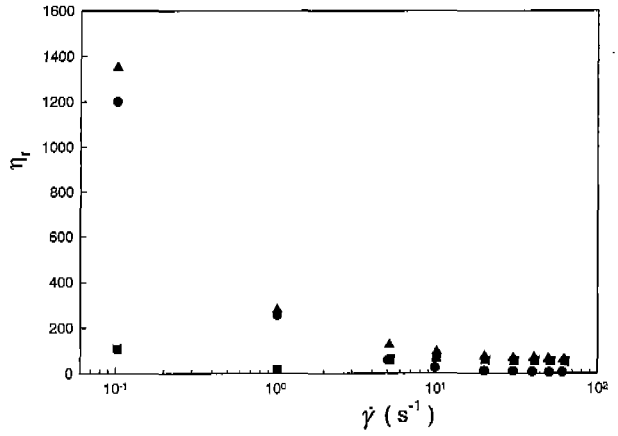

Fig. 3. Shear rate dependence of the different contributions to the relative viscosity of a polymethylmethacrylate particle suspension of 0.547 volume fraction. (Data adapted from Kaffashi *et al.*, 1997), ▲; η_r total, ●; η_r elastic-like, ■ ; η_r viscous.

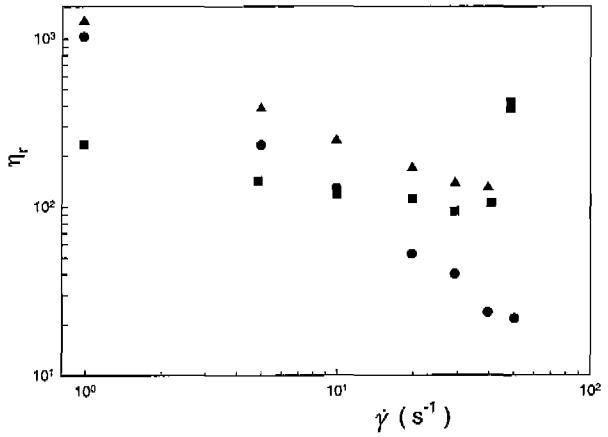

Fig. 4. Shear rate dependence of the different contributions to the relative viscosity of a silica particle suspension of 0.59 volume fraction. (Data adapted from O'Brien and Mackay 2000), ▲; η_r total, ●; η_r elastic-like, ■; η_r viscous.

studied. There was good agreement between this time constant and that from diffusion of a single particle. Kaffashi *et al.* (1997) also pointed out the similarity of the stress decay and fractal diffusion of particles.

More recently, O'Brien and Mackay (2000) studied the rheological properties, especially shear thickening, of concentrated silica hard sphere suspensions. The charged silica particles were coated with 3-(trimethoxysilylpropyl) methacrylate (TPM) and dispersed in tetrahydrofurfuryl alcohol (THFFA) using centrifugation. The particles were essentially monodisperse with a diameter of 140 nm, determined via SEM. Three volume fractions of 0.54, 0.59 and 0.63 were produced. The measurements were performed with a 50 mm diameter cone and plate geometry of a cone angle of 0.0874 rad. All three volume fractions were believed to be above the glass transition volume fraction (that is: the material exhibits solid behavior), based on the observations that no zero shear rate viscosity existed and stress decay followed power law dynamics which suggested a fractal-like microstructure. The elastic-like viscosity component decreased with shear rate while the viscous viscosity component remained almost constant at low shear rate. The highest volume fraction, 0.63, was dominated by the elastic-like stress while the lowest one, 0.54, was dominated by the viscous stress. Different behaviors were observed when shear thickening was involved. The lowest volume fraction showed continuous shear thickening, as gradually increasing steady viscosity values were measured. For the samples with volume fractions 0.59 and 0.63, discontinuous shear thickening was observed, i.e., at a critical shear rate, the stress rose rapidly and did not achieve a steady state value. Relative viscosity versus shear rate for the 0.59 volume fraction is shown in Fig. 4. Moreover, the type of shear thickening changed as well. For the two lower volume fractions, shear thickening was attributed to the increase in the viscous component of viscosity. It was consistent with the simulations (Foss and Brady, 2000) and the optical measurements (Bender and Wagner, 1995) on similar systems, confirming that shear thickening in such suspensions is caused by particle clustering. For the highest volume fraction sample, shear thickening was associated with an increase in the elastic component. This can also be interpreted via the clustering theory (Bender and Wagner, 1995). As clustering caused an increase of the effective volume fraction, O'Brien and Mackay (2000) argued that the highest volume fraction, 0.63, caused the effective volume fraction to reach a maximum packing value and thus the sample became solid-like in nature.

2.5. Stress-optical measurements

The stress-optical law for polymers was extended by Bender and Wagner (1995) to colloidal suspensions. As the birefringence index of polymer solutions provided a direct measurement of the entropic (elastic-like) force, the authors established a similar relationship equating measurements of the complex refractive index tensor to the measurements of the thermodynamic contribution to the stress tensor. In a shear flow, the relation is given as:

$$\Delta n''_{45^\circ} = C\sigma^{thermo} \tag{3}$$

where $\Delta n''_{45^\circ}$ is the magnitude of the dichroism measured at a 45° angle to the flow-direction in the flow-velocity-gradient plane, σ^{thermo} is the thermodynamic contribution to the stress and C is a stress-optical coefficient, depending on particle size, volume fraction, wavelength of the light, the refractive index difference between the particles and the medium, and potentially on the Peclet number. Since the shear stress consists of the thermodynamic contribution and the hydrodynamic contribution:

$$\sigma = \sigma^{thermo} + \sigma^{hydro} \quad (4)$$

the combination of rheological and flow dichroism measurements yields a method to distinguish between the elastic-like stress (thermodynamic) and viscous stress (hydrodynamic). Strictly speaking, the stress-optical relationship for suspensions is valid only in the linear limit, i.e. for asymptotically low shear rates. However, for concentrated suspensions of charged particles, as well as for hard-spheres and sterically stabilized suspensions, Equation (3) can be considered to be approximately correct.

The systems studied by Bender and Wagner (1995) were hard sphere silica particle suspensions. The monodisperse particles were produced following the Stober process (Stober *et al.*, 1968), involving the condensation reaction of tetraethylorthosilicate (TEOS) in the presence of a base (NH_3) at room temperature. Particles of three diameters (labeled as HS100, HS200 and HS400) were obtained by varying the concentration of base and of TEOS. The diameters were 95 nm, 140 nm and 400 nm respectively, determined via TEM. To provide near hard sphere character, particles were coated with 3-(trimethoxysilylpropyl) methacrylate (TPM) to remove surface charges and index-matched in tetrahydrofurfural alcohol (THFA) to provide an optically transparent suspension and to remove Van der Waals interaction. A variety of volume fractions were obtained by diluting a stock suspension. Viscosities were measured on a Bohlin CS10 controlled-stress rheometer with a 4° cone-and-plate geometry and the dichroism of the shearing suspensions was measured with a Rheometrics Rheo-optic Analyzer (ROA). An example data set, plotted as stress versus shear rate, for HS200 at a volume fraction of 0.52 is shown in Fig. 5. The authors found that the viscous viscosity component was constant throughout the shear thinning regime. Bender and Wagner (1996) observed that the hydrodynamic stress dominated the shear thickening region in their investigation of the shear thickening behavior of the silica suspensions with the same rheo-optical technique, justifying the clustering theory.

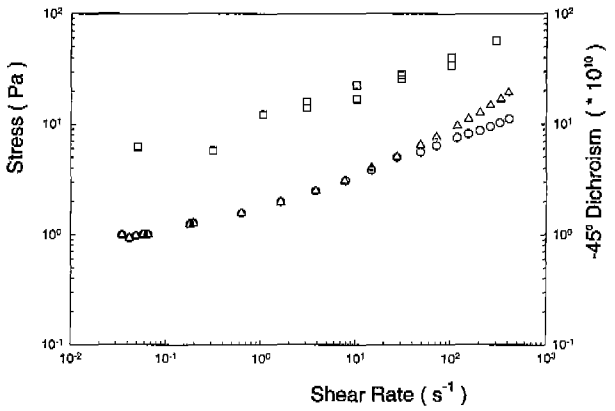

Fig. 5. Total shear stress, dichroism and calculated elastic-like stress versus shear rate for a silica particle suspension of 0.52 volume fraction. (From Bender and Wagner, 1995, reprinted with permission from Wagner), □; dichroism, △; total shear stress, ○; calculated elastic-like stress.

2.6. Rigid molecules

Mackay and Liang (1992) reported stress jump measurements of semidilute solutions of rigid molecules (Tobacco Mosaic Virus (TMV)) in shear flow. The virus was isolated from infected plant leaves after sufficient growing time. The concentration in the buffer solution was determined by optical density measurements. Further adjustments were performed to produce a solvent consisting of 75 wt.% fructose and 25 wt.% buffer solution. The length of the virus was found to be 690± 469 nm and the diameter was 18± 4 nm, determined via scanning electron micrographs. The solvent density was measured to be 1374 kg/m^3 at 22°C and the TMV density was assumed to be 1370 kg/m^3. A variety of concentrations were used, from 2.4 mg/ml to 21.6 mg/ml and the experiments were run on a modified Rheometrics RFS rheometer at 22°C. Steady shear measurements revealed that, the shear rate range from 0.001 s^{-1} to 200 s^{-1} was divided into three regions, one Newtonian and two shear thinning with different power indices. Stress jump measurements showed that the stress decreased to zero immediately after cessation of flow for all solutions tested in the shear rate range from 0.5 to 20 s^{-1}, indicating that the viscous contribution dominated.

Liquid-crystal polymers (LCPs), exhibiting unique rheological properties, have been actively studied in the past five decades. The viscous contribution is frequently ignored by most theories. To verify the existence of a viscous stress in LCPs, Smyth and Mackay (1994) performed a series of rheological measurements on lyotropic aqueous hydroxypropylcellulose (HPC) solutions in the biphasic and liquid-crystalline regions. The HPC powder came with nominal molecular weights of 100,000 Daltons. After carefully removing excess moisture, the HPC powder was mixed with distilled water in a tightly sealed and covered jar for approximately four weeks under slow rotation. Then the samples were placed in a refrigerator before testing. The experiments were performed on a Rheometrics RFS-8400 rheometer at room temperature (23± 2°C) with a cone and plate geometry of diameter 25 mm and an angle of 0.09985 rad, and on a RDS II rheometer with a cone and plate of diameter 25 mm and an angle of 0.020 rad. The steady shear viscosity measurements suggested that solutions of concentrations above 45% were in a fully liquid-crystalline mesophase while below this concentration the solution was biphasic. Due to noise, stress jump data of shear rates below ~0.03 s^{-1} were not available. The stress jump ratio versus shear rate for various solutions are shown in Fig. 6. The general trends of the stress jump ratio showed that the viscous stress was the major component for low concen-

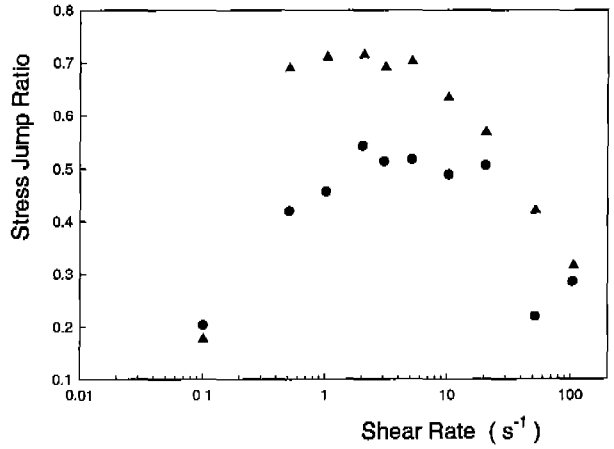

Fig. 6. Shear rate dependence of the stress jump ratio upon cessation of shear flow for two lyotropic hydroxypropylcellulose solutions. (Data adapted Smyth and Mackay, 1994), ●; 25 wt.%, ▲ ; 30 wt.%.

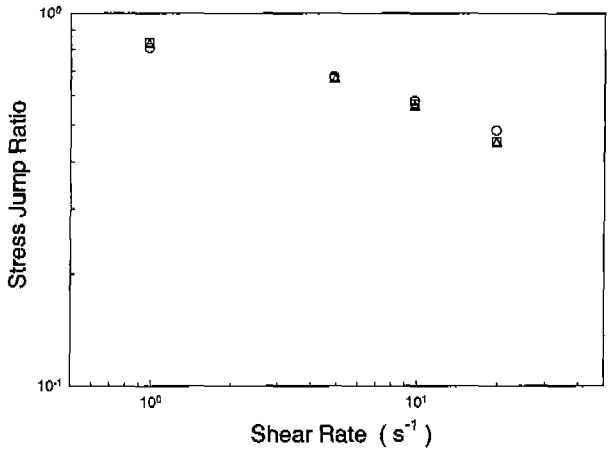

Fig. 7. Shear rate dependence of the stress jump ratio upon cessation of shear flow for three xanthan gum solutions. (Data adapted from Liang and Mackay, 1993), ○; 0.010 wt%, □; 0.020 wt%, △; 0.050 wt%.

trations at all shear rates tested, and it was dominant for all concentrations at high shear rates. An interesting observation made by Smyth and Mackay (1994) was that a local maximum was measured for stress jump ratio, which indicated that the viscous contribution reached a minimum at a critical shear rate. It is generally observed with other materials that the viscous contribution increases with shear rate, as predicted by most theories. The authors proposed an additional mechanism for viscous stress dissipation to explain this controversy. They attributed the increase of the viscous contribution with decreasing shear rate, below the critical shear rate, to the sliding of domains formed by defects in the structure, causing the dissipation of hydrodynamic energy at the interdomain boundary (the defect regions).

2.7. Polymer solutions

Liang and Mackay (1993) measured stress jump after steady shear for semidilute solutions of a semirigid xanthan gum macromolecule. The xanthan gum sample used is a polydisperse food grade commercial product manufactured by jungbunzlauer (Australia) in a solvent of 75 wt.% fructose and 25 wt.% water. Xanthan gum was first mixed with de-ionized water in a sealed bottle under slow rotation for one day, after which fructose was added and the entire solution was rotated for three more days. The solution was then allowed to rest for three days before any measurement. A variety of concentrations were prepared, from 0.005 to 0.050 wt.%. The rheological characterization was carried out on a modified Rheometrics RFS rheometer at a temperature of 22.0± 0.1°C. Two cone-and-plate geometries were used. One was 25 mm in diameter with an angle of 0.09974 rad and the other was 50 mm in diameter with an angle of 0.0874 rad. Though xanthan gum is capable of forming a liquid-crystal phase, the solutions tested by Liang and Mackay were in the semidilute region, based on the intrinsic viscosity measurements. The stress jump ratios decreased monotonically with shear rate, from around 0.8 at 1 s^{-1} to about 0.45 at 20 s^{-1}, showing the increase of the viscous contribution. The stress jump ratio versus shear rate for three solutions is shown in Fig. 7. One observed that the measured jump ratios were essentially independent of concentration. The authors postulated that there was no phase change in the samples from the dilute to semidilute region and thus no significant deviation from dilute solution behavior should be expected.

The simple linear stress-optical law, has been verified in various experimental studies on single-phase polymer melts and entangled solutions. Those studies were performed, well above the sample glass transition temperatures, under moderate chain deformation (Larson, 1999). The stress-optical law is written as:

$$\underline{\underline{n}}^{p} = C\underline{\underline{\sigma}}^{p} \tag{5}$$

where $\underline{\underline{n}}^{p}$ denotes the birefringence tensor; $\underline{\underline{\sigma}}^{p}$ is the polymer extra stress tensor and C is the stress-optical coefficient, a material constant. Some researchers (Amelar *et al.* 1991; Fuller 1995) also found the stress-optical law to be valid for dilute polymer solutions if the solvent contributions were excluded. This was not the case in the work of Smyth *et al.* (1995), who performed rheological and optical measurements on two xanthan gum solutions of 0.025 and 0.050 wt.%. The breakdown of the stress-optical law was also observed by Mead and Larson (1990) for poly(γ-benzyl L-glutamate) (PBLG) in *m*-cresol. The samples used by Smyth *et al.* were similar to those prepared in Liang and Mackay (1993) and stress jump measurements were carried out to determine the shear elastic-like and viscous stresses. It was found that the stress-optical law was valid, if only the elastic-like stress was used. This is shown in

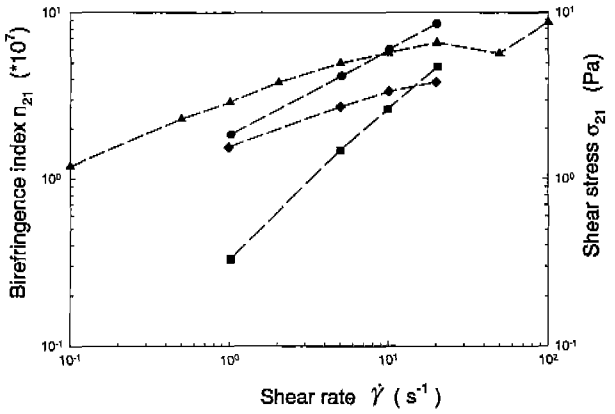

Fig. 8. The optical birefringence index versus shear rate compared with different contributions to the shear stress for a 0.05 wt.% xanthan gum solution. (Data adapted from Smyth *et al.*, 1995), ▲; n_{21}, ●; σ_{21}, ◆; σ_{21} elastic-like, ■; σ_{21} viscous.

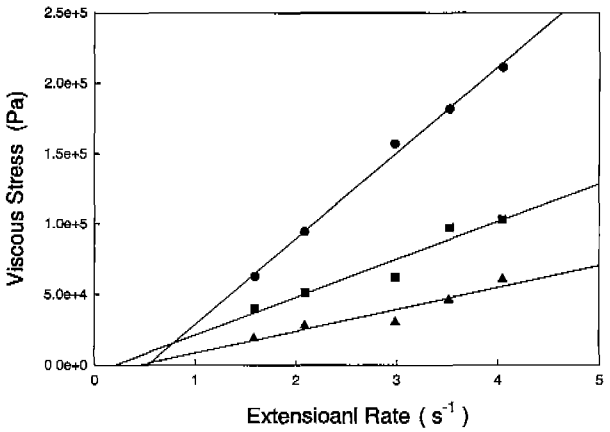

Fig. 9. Viscous stress versus extensional rate at three constant values of elastic stress for a Boger fluid. (From Orr and Sridhar 1996, reprinted with permission from Sridhar), ●; Elastic stress=58000 Pa, ■; Elastic stress=27000 Pa, ▲; Elastic stress=20000 Pa.

Fig. 8, and can be interpreted from molecular origin of the stress-optical law. The viscoelastic stresses are proportional to the second moment of the configuration distribution function in the dumbbell model and the network model. Mechanical viscoelastic stresses can be interpreted in terms of anisotropy in molecular orientations and thus a proportionality may exist between the polymer viscoelastic stress and the optical anisotropy or birefringence (Larson, 1999). On the other hand, the viscous stress, originating from hydrodynamic interactions, has no direct and/or simple dependence on polymer configuration and may not conform to the stress-optical relationship.

2.8. Elongational stress jump

While Mackay and coworkers were performing direct measurements of stress jump in shear flow, others (Orr and Sridhar, 1996; Spiegelberg and McKinley, 1996) also discovered stress jump in extensional flow.

Orr and Sridhar (1996) investigated the nature of extensional stresses by performing stress relaxation measurements following extensional deformation. In a typical relaxation experiment, a rapid stress decrease could be observed followed by a slow stress relaxation. However, the rapid change of velocity of the platform could cause the initial stress relaxation to oscillate. The authors used the sum of two exponentials (see Equation (6)) to fit the residual stress time curve.

$$\sigma = A\exp(-t/a)+B\exp(-t/b) \quad (6)$$

The stress at $t = 0$ was then obtained from Equation (6). This stress was considered to be the elastic stress and the difference between the stress measured at (total stress) and the elastic stress was taken to be the viscous stress. The samples studied were two PIB Boger fluids, labeled as Fluid A (0.31 wt.% PIB, 94.86 wt.% PB and 4.83 wt.% tetradecane) and Fluid B (0.185 wt.% PIB, 92.37 wt.% PB and 7.45 wt.% kerosene) with molecular weights of 1.2×10^6 and 2.4×10^6 and viscosities at 21.5°C of 19 Pa·s and 34.2 Pa·s respectively.

Because a finite time was needed to stop stretching (frequently assumed to happen instantaneously in stress relaxation), Orr and Sridhar (1996) studied the effect of the deceleration rate of the rheometer on stress relaxation. They found that once the time frame was appropriately offset, such that the moments at which the rheometer came to complete rest coincided for each experiment, the rate of the initial rapid stress decrease was proportional to the rate at which the rheometer was decelerated. The residual stresses then merged and started a slow relaxation. This supported the hypothesis that the initial stress decrease was due to viscous dissipation. Stress relaxation measurements after steady state showed that, the elastic stress was independent of elongational rate. The authors stated that this result was due to the fact that the contour length of the macromolecule was identical for each elongational rate at steady state. On the other hand, a linear relation was found between the viscous stress and the elongational rate at constant elastic stress values, as shown in Fig. 9. That is to say: the viscous extensional viscosity was constant. The authors also performed relaxation measurements prior to reaching steady state, to determine the transient stress. That is: to determine the viscous stress growth and the elastic stress growth. It was found that the transient viscous stress increased faster with time than the elastic one. The transient viscous stress was observed to be proportional to the strain rate at any constant value of elastic stress, and hence chain extension. A log-log plot of the viscous contribution of the extensional viscosity versus elastic stress displayed a linear dependence on the elastic component. Based on these observations, Orr and Sridhar (1996) proposed a

mathematical relationship between the viscous and the elastic stress such that:

$$\sigma^{v} = k\dot{\varepsilon}\{\sigma^{e}\}^{\alpha} \tag{7}$$

where σ^{v} and σ^{e} represents the viscous and elastic extensional stress respectively, k and α are constants, $\dot{\varepsilon}$ is the extensional rate.

Spiegelberg and McKinley (1996) studied the extensional behavior of three polystyrene-based Boger fluids, using a filament stretching rheometer of a similar design to that by Tirtaatmadja and Sridhar (1993). The PS with molecular weight of 2.25×10^{6} was dissolved in oligomeric styrene at concentrations of 0.05, 0.1 and 0.2 wt.% respectively. They also observed a rapid initial decrease of the tensile stress upon flow cessation followed by a slow stress decay. The magnitude of the decrease increased with extension rate. One could interpret this as resulting from dissipative stresses associated with frictional drag.

2.9. Theoretical modeling

2.9.1. Oldroyd B model

As mentioned earlier, the linear Jeffreys model is able to predict the stress discontinuity at cessation of flow. Its non-linear counterpart, the convected Jeffreys model or Oldroyd B model, contains the same characteristics, and can be written as (Bird *et al.*, 1987):

$$\underline{\underline{\sigma}} + \lambda_1 \overset{\nabla}{\underline{\underline{\sigma}}} = -\eta_0\left(\underline{\underline{\dot{\gamma}}} + \lambda_2 \overset{\nabla}{\underline{\underline{\dot{\gamma}}}}\right) \tag{8}$$

where $\underline{\underline{\sigma}}$ and $\underline{\underline{\dot{\gamma}}}$ are the extra stress tensor and the strain rate tensor respectively; $\overset{\nabla}{}$ refers to the upper convected derivative. The three model parameters are: λ_1, the relaxation time, η_0 the zero shear viscosity and λ_2 the retardation time. At steady shear flow, the elastic and the viscous components of the viscosity are:

$$\eta^{e} = \frac{\lambda_1-\lambda_2}{\lambda_1}\eta_0, \qquad \eta^{v} = \frac{\lambda_2}{\lambda_1}\eta_0 \tag{9a, b}$$

For steady uniaxial extensional flow, these components are:

$$\eta_E^{e} = \frac{3(\lambda_1-\lambda_2)\eta_0}{\lambda_1(1+\lambda_1\dot{\varepsilon})(1-2\lambda_1\dot{\varepsilon})}, \qquad \eta_E^{v} = 3\frac{\lambda_2}{\lambda_1}\eta_0 \tag{9c, d}$$

However, as seen in the molecular counterpart of Equation (8), the elastic Hookean dumbbell model (Bird *et al.*, 1987), the viscous stress is related exclusively to the purely viscous hypothetical solvent. Note that, this hypothetical solvent contribution may not be equivalent to the actual measured viscosity of the solvent in a real system.

Mackay *et al.* (1989) reported a shear stress jump due to the solvent for a dilute solution of PIB in a viscous solvent consisting of kerosene and a low molecular weight poly(1-butene). This type of discontinuity, as indicated by Liang and Mackay (1993), tells little of the polymer dynamics.

2.9.2. Bird-Curtiss model

Curtiss and Bird (1981) presented a kinetic theory for concentrated polymers based on the phase space formalism (Bird *et al.*, 1987). The constitutive equation is given as:

$$\underline{\underline{\sigma}} = -nkT\left[\frac{1}{3}\underline{\underline{\delta}}\int_{-\infty}^{t}\mu(t-t')\underline{\underline{A}}(t,t')dt' - \zeta\int_{-\infty}^{t}\nu(t-t')\underline{\underline{B}}(t,t')dt'\right] \tag{10}$$

In this model, a linear polymeric chain, surrounded by other polymeric chains with number density n, is idealized as a Kramers freely jointed bead-rod chain, consisting of N identical beads joined by N-1 massless rigid rods. k is the Boltzmann constant, T is the absolute temperature, $\underline{\underline{\delta}}$ is the unit tensor and ζ is the link tension coefficient. μ and ν are given as:

$$\mu(t,t') = \frac{8}{\lambda}\sum_{\alpha,odd}\exp[-\pi^2\alpha^2(t-t')/\lambda] \tag{11a}$$

$$\nu(t,t') = \frac{16}{\pi^2\lambda}\sum_{\alpha,odd}\alpha^{-2}exp[-\pi^2\alpha^2(t-t')/\lambda] \tag{11b}$$

and the tensors $\underline{\underline{A}}$ and $\underline{\underline{B}}$ are:

$$\underline{\underline{A}} = \frac{1}{4\pi}\int\frac{\underline{\underline{uudu}}}{(1+\underline{\underline{\Gamma}}:\underline{\underline{uu}})^{3/2}} \tag{11c}$$

$$\underline{\underline{B}} = \frac{\lambda}{8\pi}\underline{\underline{\dot{\gamma}}}:\left(\int\frac{\underline{\underline{uuuudu}}}{(1+\underline{\underline{\Gamma}}:\underline{\underline{uu}})^{3/2}}\right) \tag{11d}$$

where λ is a time constant, $\underline{u}$ is a unit vector describing the molecular orientation; $\underline{\underline{\Gamma}}$ is the relative Cauchy-Green tensor.

The first integral in Equation (10) is configuration based and thus refers to the elastic contribution. The second integral, having a direct dependence on the flow field as seen in Equation (11d), refers to the viscous contribution. Thus the steady shear viscosity can be written as:

$$\eta = \eta_A + \varsigma\eta_B \tag{12}$$

where η_A and η_B denote the values arising from the integrals containing the tensors $\underline{\underline{A}}$ and $\underline{\underline{B}}$ respectively. The expression for the extensional viscosity can be similarly generated. Note that the link tension coefficient, ς is directly proportional to the viscous stress. This parameter determines the anisotropy of the friction tensor (Bird *et al.* 1987). If $\varsigma = 1$, the friction tensor is isotropic. If $\varsigma = 0$, there is no tension in the link. That is to say: there is no difference between the drag force on two adjacent beads and thus no stress jump exists.

The model has been successfully fitted with the shear data of polystyrene melts/solutions, polyvinyl acetate solutions and poly-α-methylstyrene solutions (Saab *et al.*, 1982), and with the extensional data of HDPE melts and polystyrene melts (Bird *et al.*, 1982).

2.9.3. De Kee-Carreau model

De Kee and Carreau (1979) proposed a model derived from Lodge's network theory. The constitutive equation is given as:

$$\underline{\underline{\sigma}} = -\int_{-\infty}^{t} m[t-t', II(t,t')]\underline{\underline{\Gamma}}dt' \tag{13}$$

where m is the memory function given by:

$$m[t-t', II(t,t')] = \sum_{p=1}^{M} \frac{\eta_p f_p[II(t')]}{\lambda_p^2} \exp\left\{-\int_{t'}^{t} \frac{dt''}{\lambda_p g_p[II(t'')]}\right\} \tag{14a}$$

η_p and λ_p are constants, f_p and g_p are functions of II, the second invariant of the deformation rate tensor, given as:

$$f_p = \exp\left[-(-2c+3)t_p\sqrt{\frac{1}{2}II}\right] \tag{14b}$$

$$g_p = \exp\left[-(c-1)t_p\sqrt{\frac{1}{2}II}\right] \tag{14c}$$

where the t_p are time constants and c is a dimensionless parameter.

The relation between λ_p and η_p given by Rouse is adopted and is written as:

$$\eta_p = \eta_0\lambda_p / \sum_{p=1}^{M} \lambda_p \tag{14d}$$

It is assumed that the f_p and g_p can be divided into two sets. In the first set (p=1 to k<M), t_p is non-zero, and in the second set, which can be considered to consist of only one element (p=M) with $\lambda_M \to 0$, t_p is zero. The shear viscosity is given as:

$$\eta = \sum_{p=1}^{k} \eta_p \exp(-t_p\dot{\gamma}) + \eta_\infty \tag{15a}$$

where η_∞, arising from the element in the second set as a purely viscous term, have been interpreted by Chan Man Fong and De Kee (1999), in terms of the network theory, to be the viscosity associated with the solvent molecules as well as with the dangling and stray chains. The summation term in Equation (15a) represents the elastic contribution.

In the case of steady extensional flow, the extensional viscosity is:

$$\eta_E = 3\eta_\infty + 3\sum_{p=1}^{k} \frac{\eta_p \exp(-\sqrt{3}\dot{\varepsilon}t_p)}{\{1-2\lambda_p\dot{\varepsilon}\exp[-\sqrt{3}\dot{\varepsilon}t_p(c-1)]\}\{1+\lambda_p\dot{\varepsilon}\exp[-\sqrt{3}\dot{\varepsilon}t_p(c-1)]\}} \tag{16}$$

Again the dangling and stray chains can give rise to an extensional stress jump as the $3\eta_\infty$ term will dissipate immediately upon flow cessation.

This model has been successfully fitted with the shear flow data of polystyrene solutions, polyacrylamide solutions and polyisobutylene solutions (De Kee and Carreau 1979). In addition, it has been successfully compared to shear stress jump data (Liang and Mackay, 1993) by De Kee and Chan Man Fong (1999), as shown in Fig. 10.

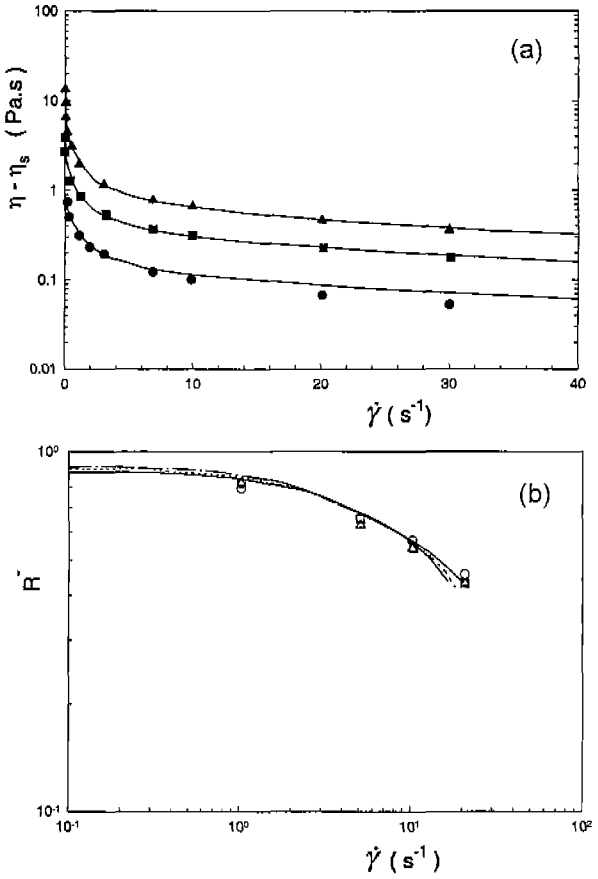

Fig. 10. (a) The polymer viscous contribution to steady-state stress versus shear rate. (b) The polymer elastic contribution to steady-state stress versus shear rate. (From Hua and Schieber, 1995, reprinted with permission from Schieber), ◆; Data from Liang and Mackay, 1993 for 0.01 wt.% xanthan gum solution, —; Predictions of the FENE dumbbell model, ----; Predictions for the Hookean dumbbell model.

2.9.4. Dumbbell model

Rigid dumbbell model

In the elastic Hookean dumbbell model, the stress due to the polymer molecules is viscoelastic while the viscous stress relates exclusively to the solvent (Bird *et al.*, 1987). That is to say, the hydrodynamic drag force acting on the beads is coupled with the elastic spring force to generate a viscoelastic force. In the rigid dumbbell model, the spring is replaced by a rigid rod which acts as constraint on the system and the hydrodynamic drag force translates to a purely viscous stress.

The Kramers expression of the stress tensor for rigid dumbbells is written as (Bird *et al.*, 1987):

$$\underline{\underline{\sigma}} = -\eta_s\underline{\underline{\dot{\gamma}}} + nkT\underline{\underline{\delta}} - 3nkT\langle\underline{u}\underline{u}\rangle - 6nk\lambda T\underline{\underline{\kappa}} : \langle\underline{u}\underline{u}\underline{u}\underline{u}\rangle \tag{17}$$

where < > stands for the average over the configuration space, η_s is the solvent viscosity and $\underline{\underline{\kappa}}$ is the transpose of the velocity gradient tensor. There also exist some other expressions for rigid dumbbells which can be transformed to each other (Bird *et al.*, 1987).

The last term in Equation (17) is the viscous contribution from the polymer, which is directly associated with the flow. The term involving the second moment of $\underline{u}$ is the elastic stress, related to the molecular configuration.

2.9.5. Bead-rod-spring model with internal viscosity

The internal viscosity was first suggested by Kuhn and Kuhn (1945), and models generated were found to be able to describe high-frequency dynamic behavior, dielectric relaxation behavior and non-linear properties (Manke and Williams, 1985). In the 1980s, the internal viscosity idea began to be associated with stress jump in the bead-rod-spring molecular model.

The expression for the connector force between two adjacent beads, when an internal viscosity is considered, is written as (Manke and Williams, 1986):

$$\underline{F}^c = H\underline{Q} + \varphi\left(\frac{\underline{Q}\cdot\dot{\underline{Q}}}{\underline{Q}^2}\right)\underline{Q} \tag{18}$$

where H is the Hookean spring constant, φ is the internal viscosity coefficient, $\underline{Q}$ is the end-to-end vector of a dumbbell and $\dot{\underline{Q}}$ is the time derivative of $\underline{Q}$. It is equivalent to that of a dashpot connected in parallel with a spring. This dashpot force resists fast change of bead separation and represents a viscous contribution to the total stress.

When Equation (18) is used, non-linear and higher order terms of $\underline{Q}$ will appear in the expression for the stress tensor. If the Kramers dumbbell equation is used (Bird *et al.* 1987), the stress due to the polymers can be written as (Wedgewood, 1993):

$$\underline{\underline{\sigma}}_p = nkT\left\{\underline{\underline{\delta}} - 3g\left\langle\frac{\underline{\underline{QQ}}}{\underline{Q}^2}\right\rangle\right\} - nH(1-g)\langle\underline{Q}\underline{Q}\rangle - \frac{n\zeta g}{2}\underline{\underline{\kappa}}:\left\langle\frac{\underline{\underline{QQQQ}}}{\underline{Q}^2}\right\rangle \tag{19}$$

where g is a parameter associated with the internal viscosity coefficient and ζ is the Stoke's drag coefficient. Suitable approximation methods have to be adopted in order to achieve closure. A lot of work has been done on modeling polymer molecules with internal viscosity (Manke and Williams, 1992; Schieber, 1993; Wedgewood, 1993; Sureshkumar and Beris, 1995, to name a few). Depending on the simplification method as well as on some other issues (such as hydrodynamic interaction) used in the theory, one may reach different results. Once internal viscosity is considered, the bead-rod-spring model is able to predict stress jump as revealed by Equation (19). The last term on the right side is associated with the velocity gradient tensor and is thus associated with the purely viscous contribution. The quantity represented by the last term will dissipate immediately as the velocity field is set to zero, in either shear or extensional flow.

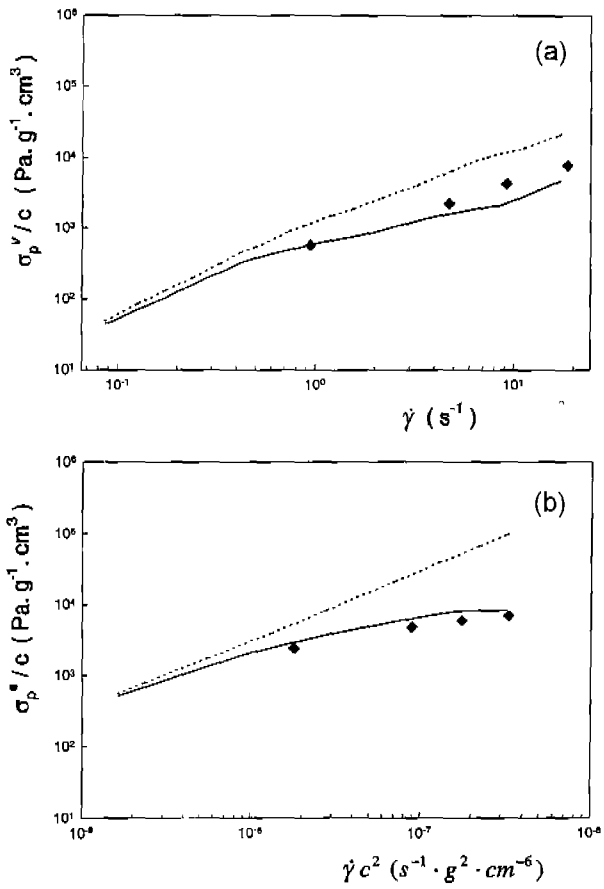

Fig. 11. (a) Viscosity excluding solvent contribution (η-η_s) versus shear rate from three xanthan gum solutions. (Reprinted from De Kee and Chan Man Fong, 1999), Data from Liang and Mackay (1993): ▲; 0.050 wt%, ■; 0.020 wt%, ●; 0.010 wt.%, —; Predictions of the De Kee-Carreau model.
(b) Stress jump ratio upon cessation of flow versus shear rate for three xanthan gum solutions. Data from Liang and Mackay (1993): ○; 0.010 wt%, □; 0.020 wt%, △; 0.050 wt%, Predictions of the the De Kee-Carreau model: —; 0.010 wt%, ----; 0.020 wt.%, -·-·; 0.050 wt.%.

Schieber (1993) studied an internal viscosity Hookean dumbbell model with a Gaussian distribution function approximation. He successfully compared the model predictions with the stress jump data of Liang and Mackay (1993). Hua and Schieber (1995) used non-equilibrium Brownian dynamics simulations to investigate the flow behavior of Hookean and FENE dumbbells with internal viscosity. Here also, reasonable agreement with the viscous and elastic stress on a xanthan gum solution (Liang and Mackay, 1993) was obtained as shown in Fig. 11.

2.9.6. Liquid crystal polymers

In general, polymer molecules that generate liquid-crystalline solutions or melts are semirigid or contain rigid units named mesogens. The isotropic-to-nematic transition

is accompanied by a viscosity drop, resulting from less resistance for polymer molecules to slide over each other in an ordered state than in an isotropic state (Larson, 1999). The shearing of LCPs is usually characterized by three regions: one shear-thinning at low shear rate (Region I) and a second shear-thinning at high shear rate (Region III), plus a Newtonian plateau at intermediate rate (Region II). However, for some polymers, Region I has not yet been observed. Another special property of some nematic LCPs is the observation of a negative primary normal stress coefficient in a certain shear rate range.

For oriented rod-like polymer solutions, the stress tensor is given by (Doi and Edwards, 1986; Larson, 1999):

$$\underline{\underline{\sigma}}_p = 3nkT\langle \underline{u}\underline{u} - \frac{1}{3}\underline{\underline{\delta}}\rangle + n\left\langle \left(\frac{\partial}{\partial \underline{u}} U_{nem}\right)\underline{u}\right\rangle + n\zeta \underline{\underline{\kappa}} : \langle \underline{u}\underline{u}\underline{u}\underline{u}\rangle \tag{20}$$

where U_{nem} is the nematic potential. The first term in Equation (20) is due to Brownian motion and the last term is due to the viscous drag force on the polymer.

Smyth and Mackay (1994) interpreted current theories on LCPs and found a discrepancy with their measured data on aqueous hydroxypropylcellulose solutions in liquid-crystalline mesophase. According to Doi (1981), Marrucci and Maffettone (1989), Larson (1990) and Marrucci (1991), the elastic stress consists of three components: molecular orientation, interaction potential and director distortion, all of which are specified as functions of the rod orientation vector $\underline{u}$, while the hydrodynamic stress is expressed in terms of the double dot product of the deformation rate tensor and the fourth moment of $\underline{u}$. The viscous stress should be insignificant at low shear rate so that the stress jump ratio tends to one with decreasing shear rate. However, a local maximum of the stress jump ratio was obtained in the experiment. In addition, as calculated by Liang and Mackay (1993) based on current theories, the stress jump ratio should show a strong concentration dependence which was not observed in the experiment. Smyth and Mackay (1994) then proposed a fifth contribution to the stress: the dissipative domain sliding force, similar to that in superplastic materials which may be deformed to a remarkable extent at a low rate due to the sliding of grains. The required grain size for superplasticity to happen is of the same order as the domain size of the LCPs. This sliding mechanism cannot exist at high rates where failure may occur. This may explain why the viscous contribution increases with decreasing rate at low shear rate.

2.9.7. Network model with internal viscosity

Sun (2000) and Sun *et al.* (2000b) introduced the idea of internal viscosity into a transient non-affine network model. The expression for the total stress tensor is given by (Bird *et al.*, 1987):

$$\underline{\underline{\pi}} = \langle \underline{Q}\underline{F}^c \rangle \tag{21a}$$

where the connector force is assumed to be given by Equation (18) and

$$\underline{\underline{\pi}} = \underline{\underline{\sigma}} + p\underline{\underline{\delta}} \tag{21b}$$

where p is the static hydrodynamic pressure. The network segments are assumed to move non-affinely such that:

$$\dot{\underline{Q}} = [\underline{\underline{\kappa}} \cdot \underline{Q}] - \frac{1}{2}\xi[\dot{\underline{\underline{\gamma}}} \cdot \underline{Q}] = \hat{\underline{\underline{\kappa}}} \cdot \underline{Q} \tag{22}$$

where ξ is a slip parameter. Combining Equations (21) and (22) yields:

$$\underline{\underline{\pi}} = -H\langle \underline{Q}\underline{Q}\rangle - \varphi \hat{\underline{\underline{\kappa}}} : \langle \frac{\underline{Q}\underline{Q}\underline{Q}\underline{Q}}{Q^2}\rangle \tag{23}$$

Through suitable approximations, the final constitutive equation is written as:

$$\underline{\underline{\pi}}^e + \lambda \overset{\square}{\underline{\underline{\pi}}}^e = -\frac{\eta_m}{\lambda(1-\xi)}\underline{\underline{\delta}} \tag{24a}$$

$$\underline{\underline{\pi}} = \underline{\underline{\pi}}^e + \varepsilon \frac{\hat{\underline{\underline{\kappa}}} : \underline{\underline{\pi}}^e \underline{\underline{\pi}}^e + (1-\xi)\underline{\underline{\pi}}^e \cdot \dot{\underline{\underline{\gamma}}} \cdot \underline{\underline{\pi}}^e}{tr(\underline{\underline{\pi}}^e)} \tag{24b}$$

where $\varepsilon \left(= \frac{\varphi}{H}\right)$, the internal parameter, as well as λ and η_m, are functions of the second invariant of the deformation rate tensor, $tr(.)$ is the trace of the tensor and $\overset{\square}{\underline{\underline{\pi}}}$ is the Gordon-Schowalter derivative of the total stress tensor:

$$\overset{\square}{\underline{\underline{\pi}}} = \frac{\partial \underline{\underline{\pi}}}{\partial t} + (\underline{v} \cdot \underline{\nabla})\underline{\underline{\pi}} - \underline{\underline{\kappa}} \cdot \underline{\underline{\pi}} - \underline{\underline{\pi}} \cdot \underline{\underline{\kappa}}^+ + \frac{\xi}{2}[\dot{\underline{\underline{\gamma}}} \cdot \underline{\underline{\pi}} + \underline{\underline{\pi}} \cdot \dot{\underline{\underline{\gamma}}}] \tag{25}$$

$\underline{\underline{\pi}}^e$, the elastic contribution, will relax gradually upon cessation of flow, conforming to Equation (24a). The second term on the right side of Equation (24b), having an explicit dependence on the flow field, is the viscous contribution and is proportional to the internal viscosity coefficient. The exact meaning of internal viscosity is not yet clear. Some (Schieber, 1993; Wedgewood, 1993) attribute the internal viscosity to the internal friction of gauche/trans rotations along the polymer backbone that have energy barriers (de Gennes, 1979), and friction between two segments of the polymer chain which are far away along the backbone but near in space (Fixman, 1988). The latter force may diminish with shear since polymer chains will stretch along the flow field. This adds to the complexity in formulating an internal viscosity model. Equation (18) is not the only tested formulation for the internal viscosity. Zimmerman and Williams (1973) summarized four versions of the internal viscosity models with respect to their ability to fit experimental data. Those four models evolved mainly from the formulas of the internal viscosity force proposed by Cerf (1957; 1958; 1969), which was proportional to the deformational velocity of the beads. The evaluation of the deformational velocity depended on an angular rotation rate and was controversial. It would either lead to an asym-

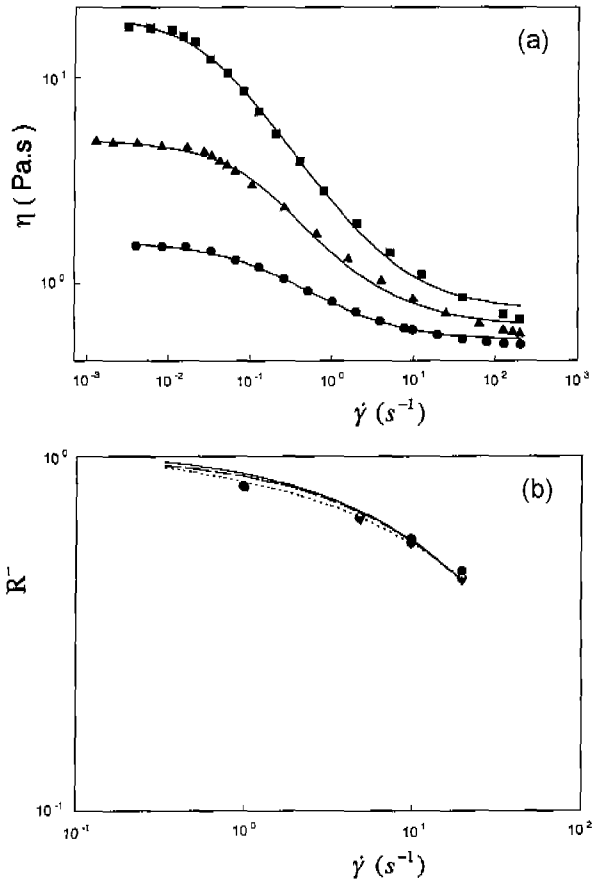

Fig. 12. (a) Steady shear viscosity versus shear rate for three xanthan gum solutions. (Reprinted from Sun *et al.*, 2000b), Data from Liang and Mackay (1993): ■; 0.050 wt.%, ▲, 0.020 wt.%, ●; 0.010 wt.%, —; Predictions of the network model with internal viscosity.
(b) Stress jump ratio upon cessation of flow versus shear rate for three xanthan gum solutions. (Reprinted from Sun *et al.*, 2000b), Predictions of the network model with internal viscosity, —, 0.010 wt.%, ---; 0.020 wt.%, ——; 0.050 wt.%.

metric stress tensor, or after imposing a "symmetrized function", yield a limited range of viscosity predictions. These models are no longer used. Schieber (1992) examined several dumbbell models with an internal viscosity force and proved that the model with the formulation given by Equation (18) satisfies an explicitly stated interdependence of the fluctuating and dissipative forces, known as the fluctuation-dissipation theorem.

Our recent model (Sun *et al.*, 2000b) predicts a stress jump in both shear flow and extensional flow. Successful model comparisons with experimental data on the shear viscosity and shear stress jump of xanthan gum solutions (Liang and Mackay, 1993) are shown in Fig. 12. In addition, our modified transient network model with internal viscosity was found to adequately describe a variety of shear material functions, such as non-Newtonian shear viscosity, primary normal stress coefficient, stress growth as well as the components of the complex viscosity. Model predictions were compared with data on xanthan gum solutions, a LDPE melt and polyacrylamide solutions.

2.10. Discussion

There have been many constitutive equations developed for various systems. However, basic criteria by which one may select the most useful rheological equation are not available. It is highly desirable that a model can describe as many material functions as possible. The existence of a stress jump directly affects the material transient behavior and thus a successful model should be able to predict such a discontinuity. A variety of theoretical models are summarized in this contribution, and listed in Table 1. Liang and Mackay (1993) have also provided a very good review.

A stress jump may originate from a purely viscous solvent contribution such as in the Oldroyd B model or from the intermolecular interaction (friction between solvent molecules and macromolecules). Intermolecular interaction is reflected in the Bird-Curtiss model, the De Kee-Carreau model and in the rigid dumbbell model. A stress jump may also originate from the intramolecular interaction (the friction between different segments of a macromolecular chain), such as in the dumbbell model and network model with internal viscosity. The comparison work supports both of these mechanisms and the measured polymer viscous stress may be due to either one or both. Because of the limited experimental data available, it is hard to assert which model is superior at this time. In addition, more compar-

Table 1. Constitutive equation-mechanism relation

Model	Theoretical Base	Characteristic Equations	Stress Jump Force
Oldroyd-B	Elastic dumbbell	Eq.(8)	Solvent contribution
Bird-Curtiss	Phase space	Eq.(10)	Intermolecular friction
De Kee-Carreau	Network type	Eqs.(13), (14)	Intermolecular friction
Rigid dumbbell	Dumbbell type	Eq. (17)	Intermolecular friction
Dumbbell with IV	Dumbbell type	Eq. (19)	Intramolecular friction
LCP	Rod-like polymers	Eq. (20)	Intermolecular friction
Network with IV	Network type	Eq. (24)	Intramolecular friction

ison work between model predictions and experimental data (including birefringence measurements) is yet to be done. When selecting a model, it is important to identify those models which are based on a sound theoretical foundation. It is also important for a model to be able to predict several material functions in terms of a small number of model parameters. In their review of useful rheological equations, Carreau and De Kee (1979) showed that the models obtained from molecular network considerations appear to be the most successful equations. The modified network model by Sun *et al.* (2000b) is able to describe a variety of material functions, including steady shear functions, linear viscoelasticity, stress growth as well as the stress jump ratio, with a reasonable number of model parameters. An improvement of elongational viscosity predictions via the network model has also been shown by Sun *et al.* (2000a).

2.11. Conclusions

The stress jump measurement provides a direct way to distinguish between the viscoelastic and purely viscous stresses. The viscous stress, dissipating instantaneously at the moment of cessation of flow, can be captured by modified rheometers. Basically, the analog filter installed in a rheometer for noise filtering is shorted out or modified so that the high frequency stress jump signal can be recorded. However, it is impossible to directly measure the dissipated stress value. Current technology, via extrapolation based on reliable transient data, provides an indirect evaluation method. Such extrapolations, in the absence of reliable data for the short period following the cessation of flow, may be subject to errors. Remmelgas *et al.* (1998) compared the elongational transient data of Orr and Sridhar (1996) to the prediction of the FENE-CR model. Due to the increasing stiffness of the nonlinear spring with chain extension, they found that the purely viscoelastic FENE-CR model predicted an apparent viscous stress if the extrapolation procedure was applied. That is to say, the measured rapid initial stress decrease of the Boger fluids by Orr and Sridhar (1996) might not be due to viscous dissipation. Based on the reasonable agreement between the model predictions and the experimental data, Remmelgas et al. (1998) concluded that the rapid initial stress decrease was most likely due primarily to the nonlinear dependence of the viscoelastic stress. It is recognized that in the shear flow test, it takes 1-5 ms for the motor to stop. Data collected in the first 15-20 ms are scattered and are ignored (Liang and Mackay, 1993). In the extensional flow test, it takes at least 50 ms for the motor to stop (Orr and Sridhar, 1996). Any viscoelastic stress with relaxation time less than those mentioned above cannot be distinguished from the viscous stress. Theoretically speaking, the stress jump ratio measured in experiments represents an upper limit for the viscous stress. A more accurate evaluation relies on the development of instrumental techniques.

The stress-optical rule states that the birefringence index is proportional to the viscoelastic stress (Fuller, 1995). Liang and Mackay (1993) did not observe a stress jump for a variety of polymer melts tested in their laboratory, suggesting the fact that polymer melts are dominated by viscoelastic stress. For semirigid and rigid macromolecular solutions, as well as for hard sphere suspensions, the "viscoelastic" component of viscosity (a decreasing function of shear rate) , dominates the viscous component at low shear rate. The viscous stress becomes prominent at high shear rate.

Another interesting issue concerns the normal stress jump. Note that, we refer here to the primary normal stress difference $N_1(=\sigma_{11}-\sigma_{22})$ or the primary normal stress coefficient $\psi_1(=-N_1/\dot{\gamma}^2)$. Currently there is no experimental evidence proving the existence of such a normal stress jump and various models may generate different predictions. For example, at cessation of flow, the Bird-Curtiss model predicts a normal stress jump. So do the De Kee-Carreau model and the bead-rod-spring model with internal viscosity (Manke and Williams, 1989). De Kee and Chan Man Fong (1999) showed that a non-zero primary normal stress coefficient at infinite shear rate $\psi_{1\infty}$ should exist for a normal stress jump to occur. The experimental work of Choe (1993) suggests such non-zero $\psi_{1\infty}$. The network model with internal viscosity by Sun *et al.* (2000b) predicts no normal stress jump. It is possible that there is no normal stress jump, as the jump characteristics are most likely related to the purely viscous contribution. This conflict is yet to be solved.

References

Amelar, S., C. E. Eastman, R. L. Morris, M. A. Smeltzly, T. P. Lodge and E. D. von Meerwall, 1991, *Macromolecules* **24**, 3506.

Bender, J. W. and N. J. Wagner, 1995, Optical measurement of the contributions of colloidal forces to the rheology of concentrated suspensions, *J. Colloid Int. Sci.* **172**, 171-184.

Bender, J. W. and N. J. Wagner, 1996, Reversible shear thickening in monodisperse and bidisperse colloidal dispersions, *J. Rheol.* **40**, 899-916.

Bird, R. B., H. H. Saab and C. F. Curtiss, 1982, A kinetic theory for polymer melts. 3. Elongational flows, *J. Phys. Chem.* **86**, 1102-1106.

Bird., R. B., C. F. Curtiss, R. C. Armstrong and O. Hassager, 1987, in Dynamics of Polymeric Liquids, v. 2 Kinetic Theory, 2nd Ed., John Wiley & Sons, New York.

Cerf, R., 1957, La macromolecule en chaine dans un champ hydrodynamique theorie generale proprietes dynamo-optiques, *J. Polymer Sci.* **23**, 125-150.

Cerf, R., 1958, Mecanique statistique des macromolecules en chaines dans un champ de vitesses, *J. Phys. Radium* **19**, 122-134.

Cerf, R., 1969, Sur la theorie des proprietes hydrodynamiques des solutions de macromolecules en chaines, *J. Chim. Phys.* **66**, 479-488.

Chan Man Fong, C. F. and D. De Kee, 1999, Advances in the Flow and Rheology of Non-Newtonian Fluids, D. A. Siginer, D. De Kee and R.P. Chhabra, Eds., Elsevier, Amsterdam.

Choe, J. H., 1993, High-shear-rate measurements of the first normal stress difference N1 and viscosity for solutions of narrow distribution polystyrene in dioctyl phthalate, Ph.D. thesis, University of Wisconsin-Madison.

Curtiss, C. F. and R. B. Bird, R. B., 1981, A kinetic theory for polymer melts. II. the stress tensor and the rheological equation of state, *J. Chem. Phys.* **74**, 2026-2033.

de Gennes, P. G., 1979, Scaling Concepts in Polymer physics, Cornell University, Ithaca, New York.

De Kee, D. and P. J. Carreau, 1979, A constitutive equation derived from Lodge's network theory, *J. Non-Newtonian Fluid Mech.* **6**, 127-143.

De Kee, D. and C. F. Chan Man Fong, 1999, Predictions of stress jump by a transient network model, *Macromol. Simul.* **8**, 26-28.

Doi, M., 1981, Molecular dynamics and rheological properties of concentrated solutions of rodlike polymers in isotropic and liquid crystalline phases, *J. Polym. Sci. Polym. Phys. Ed.* **19**, 229-243.

Doi, M. and S. F. Edwards, 1986, The Theory of Polymer Dynamics, Oxford, New York.

Fixman, M., 1988, Dynamics of Stiff Polymer Chains, *J. Chem. Phys.* **89**, 2442-2462.

Foss, D. R. and J. F. Brady, 2000, Structure diffusion and rheology of Brownian suspensions by Stokesian Dynamics simulation, *J. Fluid Mech.* **407**, 167-200.

Fuller, G. G., 1995, Optical Rheometry of Complex Fluids, Oxford University Press, New York.

Hua, C. C. and J. D. Schieber, 1995, Nonequilibrium Brownian dynamics simulations of Hookean and FENE dumbbells with internal viscosity, *J. Non-Newtonian Fluid Mech.* **56**, 307-332.

Kaffashi, B., V. T. O'Brient, M. E. Mackay and S. M. Underwood, 1997, Elastic-like and viscous-like components of the shear viscosity for nearly hard sphere Brownian suspensions, *J. Colloid Int. Sci.* **187**, 22-28.

Kuhn, W. and H. Kuhn, H., 1945, Bedeutung beschrankt freier drehbarkeit fur die viskositat und stromungsdoppelbrechung von fadenmoledellosungen, *Helv. Chim. Acta* **28**, 1533-1580.

Larson, R. G., 1990, Arrested tumbling in shearing flows of liquid crystal polymers, *Macromolecules* **23**, 3983-3992.

Larson, R. G., 1999, The Structure and Rheology of Complex Fluids, Oxford, New York.

Liang, C. H. and M. E. Mackay, 1993, The stress jump of a semirigid macromolecule after shear: steady-state results, *J. Rheol.* **37**, 149-174.

Mackay, M. E., 1999, personal communication.

Mackay, M. E., C. H. Liang, and C. A. Cathey, 1989, Stress jumps of dilute solutions after cessation of steady shear flow, 61st Annual Meeting of the Society of Rheology, Montreal Canada, paper II.4.14.

Mackay, M. E. and C. H. Liang, 1992, Stress jumps of tobacco mosaic virus in shear flow, in Theoretical and Applied Rheology, edited by P. Moldenaers and R. Keunings, Proc. Xith Int. Congr. on Rheology, Brussels, Belgium.

Mackay, M. E., C. H. Liang and P. J. Halley, 1992, Instrument effects on stress jump measurements, *Rheol. Acta* **31**, 481-489.

Mackay, M. E. and B. Kaffashi, 1995, Stress jumps of charged colloidal suspensions measurement of the elastic-like and viscous-like stress components, *J. Colloid Int. Sci.* **174**, 117-123.

Manke, C. W. and M. C. Williams, 1985, Internal viscosity of polymers and the role of solvent resistance, *Macromolecules* **18**, 2045-2051.

Manke, C. W. and M. C. Williams, 1986, The interval-viscosity dumbbell in the high-IV limit: implications for rheological modeling, *J. Rheol.* **30**, 19-28.

Manke, C. W. and M. C. Williams, 1987, Stress jump at the inception of shear and elongational flows of dilute polymer solutions due to internal viscosity, *J. Rheol.* **31**, 495-510.

Manke, C. W. and M. C. Williams, 1989, Transient stress and strain responses predicted by the internal viscosity model in shear flow, *J. Rheol.* **33**, 949-978.

Manke, C. W. and M. C. Williams, 1992, Stress jump predicted by the internal viscosity model with hydrodynamic interaction, *J. Rheol.* **36**, 1261-1274.

Marrucci, G. and P. L. Maffettone, 1989, Description of the liquid-crystalline phase of rodlike polymers at high shear rates, *Macromolecules* **22**, 4076-4082.

Marrucci, G., 1991, Tumbling regime of liquid-crystalline polymers, *Macromolecules* **24**, 4176-4182.

Mead, D. W. and R. G. Larson, 1990, Rheo-optical study of isotropic solutions of stiff polymers, *Macromolecules* **23**, 2524-2533.

O'Brien, V. T. and M. E. Mackay, 2000, Stress components and shear thickening of concentrated hard sphere suspensions, submitted.

Orr, N. V. and T. Sridhar, 1996, Stress relaxation in uniaxial extension, *J. Non-Newtonian Fluid Mech.* **67**, 77-103.

Remmelgas, J, L. G. Leal, N. V. Orr, and T. Sridhar, 1998, Viscous and elastic stresses in extensional rheometry, *J. Non-Newtonian Fluid Mech.* **76**, 111-135.

Saab, H. H., R. B. Bird, and C. F. Curtiss, 1982, A kinetic theory for polymer melts V. Experimental comparisons for shear-flow rheological properties, *J. Chem. Phys.* **77**, 4758-4766.

Schieber, J. D., 1992, Do internal viscosity models satisfy the fluctuationdissipation theorem? *J. Non-Newtonian Fluid Mech.* **45**, 47-61.

Schieber, J. D., 1993, Internal viscosity dumbbell model with a Gaussian approximation, *J. Rheol.* **37**, 1003-1027.

Smyth, S. F., C. H. Liang, M. E. Mackay and G. G. Fuller, 1995, The stress jump of a semirigid macromolecule after shear: comparison of the elastic stress to the birefringence, *J. Rheol.* **39**, 659-672.

Smyth, S. F. and M. E. Mackay, 1994, The viscous stress contribution to lyotropic hydroxypropylcellulose solutions in the biphasic and liquid-crystalline regions, *J. Rheol.* **38**, 1549-1558.

Spiegelberg, S. H. and G. H. McKinley, 1996, Stress relaxation and elastic decohesion of viscoelastic polymer solutions in

extensional flow, *J. Non-Newtonian Fluid Mech.* **67**, 49-76.
Stober, W., A. Fink, and E. Bohn, 1968, *J. Colloid Interface Sci.* **26**, 62.
Sun, N., 2000, The rheology of structured materials, Ph.D. thesis, Tulane University.
Sun, N., C. F. Chan Man Fong and D. De Kee, 2000a, A non-affine transient network model, *Rheol. Acta* **39**, 174-179.
Sun, N., C. F. Chan Man Fong and D. De Kee, 2000b, Network constitutive equation with internal viscosity: application to stress jump prediction, *J. Non-Newtonian Fluid Mech.* **95**, 135-146.
Sureshkumar, R. and A. N. Beris 1995, Uniformly valid approximations for the conformational integrals from Gaussian closure in the Hookean dumbbell model with internal viscosity, *J. Rheol.* **39**, 1361-1384.
Tirtaatmadja, V. and T. Sridhar, 1993, A filament stretching device for measurement of extensional viscosity, *J. Rheol.* **37**, 1081-1102.
Wedgewood, L. E., 1993, Internal viscosity in polymer kinetic theory: shear flows, *Rheol. Acta* **32**, 405-417.
Zimmerman, R. D. and M.C. Williams, 1973, Evaluation of internal viscosity models, *Trans. Soc. Rheol.*, **17**, 23-46.